Examination of Tunable Structures of Biopolymeric-synthetic Hybrid Hydrogel Microspheres Composed of Chitosan and Poly(ethylene glycol)

A thesis

submitted by

Yi Tang

In partial fulfillment of the requirements

for the degree of

Master of Science

In

Bioengineering

TUFTS UNIVERSITY

May 2016

Advisor: Hyunmin Yi

Abstract:

Controlled manufacturing of functional hydrogel microspheres with tunable mesh structures is important for many applications including biosensing, medical diagnostics and high throughput bioassays. I examined the effects of polymerizable monomer contents and inert porogens for tunable mesh sizes and polymeric network structures of functional hydrogel microspheres in this thesis. Specifically, simple micromolding fabrication scheme was utilized to manufacture uniform microspheres containing a potent aminopolysaccharide chitosan in poly(ethylene glycol) matrix. Simple fluorescent labeling and protein conjugation reactions using a rapid and bioorthogonal Tetrazine-trans-cyclooctene (Tz-TCO) cyclization reaction and a bright red fluorescent protein R-phycoerythrin (R-PE) showed tunable mesh sizes and 3D structures. Further swelling ratio and scanning electron microscopy (SEM) studies also supported the tunable fabrication of the hybrid microspheres. I expect that the findings shown in this thesis could be useful in programmable manufacturing of functional microparticles for a large range of applications.

Table of Contents

List of Figures

List of Tables

List of Equations

List of Schemes

1. Introduction

1.1 Significance

Polymeric hydrogel microparticle-based suspension arrays hold significant potential for a large number of medical diagnostic and biosensing applications as powerful alternatives to planar and bead-based arrays[1–3]. Specifically, the hydrogel arrays offer several advantages such as rapid solution-like kinetics, hydrophilic environment for ideal target-probe binding with minimal non-specific adsorption, rapid assay time and small sample volumes. Recent advances in the fabrication techniques for polymeric hydrogel microparticles have enabled convenient shape-based encoding and rapid production of complex and/or multicompartmental microparticles, opening doors for multiplexed sensing or diagnostic assays. Such techniques include stop-flow lithography[4–6], photolithography[7,8], microcapillary devices and jetting[9,10].

1.2 Challenges

Despite such advances, there exist several critical challenges in simple and programmable fabrication of polymeric hydrogel microparticles with desired properties. First, most current techniques including microfluidic methods suffer from complex equipment and the needs for delicate microflow control[4,11–13]. Second, the most commonly used polymerizable unit poly(ethylene glycol) diacrylate (PEGDA) is often not suitable for the creation of large pores that permit rapid diffusion and binding of large biomolecular targets[14,15]. Finally, the common co-polymerization technique poses challenges in preserving the biospecific affinities of the biomacromolecular probes due to the harsh radical polymerization environment[16,17]. In short summary, there exist critical needs for

simple and reliable fabrication technique to produce polymeric microparticles with controlled and tunable macroporous polymer network structures.

1.3 My approach

The approach to address these challenges in my thesis here involves simple micromolding, addition of inert PEG porogens, chitosan as a versatile aminopolysaccharide to provide an efficient conjugation handle, and polymerization-induced phase separation (PIPS). As shown in the schematic diagram of Scheme 4.1, the cross-shaped PDMS micromolds are filled with photocurable prepolymer solution containing mixtures of PEGDA, PEG600 porogen and chitosan. The addition of wetting fluid (*N*-hexadecane with photoinitiator, PI) onto the filled micromolds induces the natural formation of the droplets by surface tension between the interface of the aqueous prepolymer solution and the hydrophobic wetting fluid. Simple photopolymerization with a hand-held UV lamp (365 nm) leads the prepolymer solution to form cross-linked uniform microspheres in a controlled and low-cost manner. Within the PIPS-based core-shell structure, the chitosan is incorporated in a stable manner with chemical functionality while the PEG porogen creates macropores.

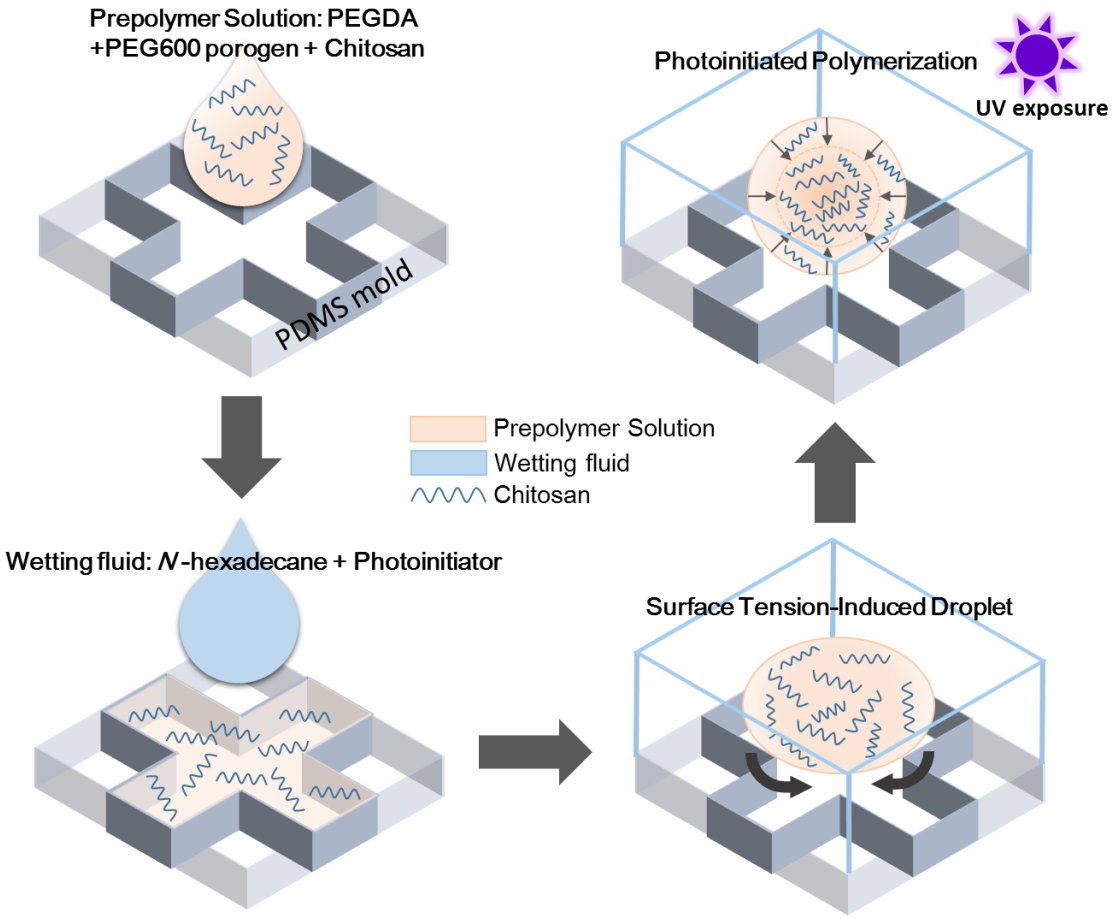

Scheme 1. Schematic diagram of the chitosan-PEG microspheres fabrication procedure, adapted from Jung and Yi[18].

1.4 Results summary

In this thesis, I built on a recent report by Dr. Sukwon Jung[18], and thoroughly examined the formation of tunable porous structures of CS-PEG microspheres. First, I used different PEGDA and PEG600 porogen conditions to examine the micromolding technique's utility towards the fabrication of uniform chitosan (CS)-PEG microspheres. Then, I examined the chemical reactivity of the incorporated chitosan by simple

fluorescent labeling. I also used confocal microscopy to further examine the spatial distribution of chitosan in the 3D structure. Afterwards, I utilized conjugation of R-PE via Tz-TCO reaction to examine the tunable macroporous structure. SEM images and diameter data are obtained to further examine the morphologies and structures of the microspheres.

2. Background:

2.1 Polymeric hydrogels

2.1.1 Radical Chain Photopolymerization

Radical polymerization is a chain reaction that can be divided into three distinct basic stages: initiation, propagation and termination[19].

As shown in Figure 2.1, initiation involves creation of the active center and usually takes place in two steps. In the first step, free radicals are created from an initiator molecules. The second step involves the addition of a free radical to a molecule of monomer.

In propagation stage, the polymer chain is growing by rapid sequential addition of monomer to the active center. Thousands of monomers are added to the chain within a few seconds.

At termination, the active center is destroyed irreversibly and the propagating polymer chain stops growing. Termination can occur by several different mechanisms, such as combination or disproportionation. For combination, two growing chains couple to form a single polymer molecule. For disproportionation, a free radical strips a hydrogen atom from an active chain, leads to the formation of two dead polymer molecules, one with a saturated end group and the other with an unsaturated end group.

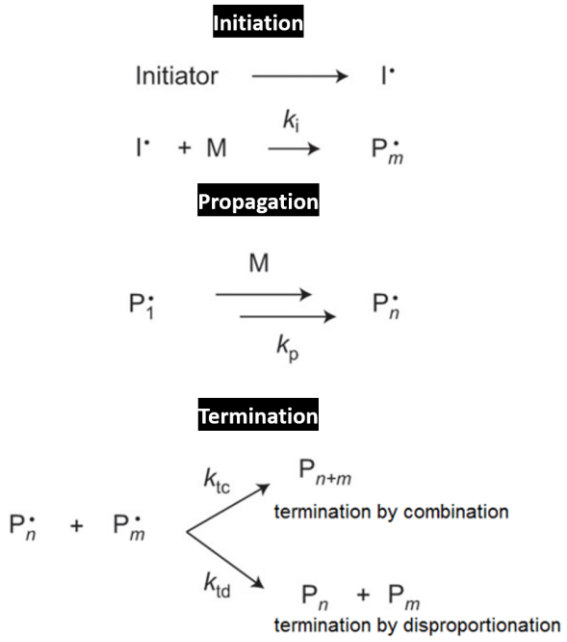

Figure 2.1. General Reaction Mechanism for Photoinitiated Radical Chain Polymerization[20].

The main advantages of photoinitiated polymerization include: (1) rapid polymerization rates (2) intense illumination (3) spatial resolution of the polymerization (4) the ability to control the initiation rates through the source of radicals, light intensity, and temperature in addition to the regions[21].

Photoinitiated chain polymerization was used for the polymeric hydrogel microspheres fabrication in Chapter 3 of this thesis.

2.1.2 Applications of Hydrogels

Hydrogels are three-dimensional networks consisting of hydrophilic polymer chains, which are crosslinked to form matrices with high water content (up to thousands of times

their dry weight)[22]. They have tunable degrees of swelling by changing the ionic strength, pH, pressure, temperature, light, electric and magnetic fields in their environment[23]. Hydrogels have gained increasing attention in biomedical field as biosensing platforms[24], drug delivery vehicles[25,26], catalyst carrier[27] and matrices for tissue engineering[26] due to their remarkable characteristic, including high biocompatibility[22], versatility in fabrication, and the stability upon the external environment[28].

2.1.3 Poly(ethylene glycol) (PEG)

Both naturally derived materials (e.g. alginates, chitosan, and dextran) and synthetic materials (e.g., poly(ethylene glycol) (PEG), poly(acrylic acid), and polyacrylamide) have been used to form biocompatible hydrogels with a three-dimensional structure characterized as a mesh[29].

Among them, PEG is a common-used polyether compound with a variety of applications due to its natural characteristics such as odorless, nonirritating, low-toxicity and water-soluble. It is widely used for water-soluble coating, thickeners, drug stabilization, fillers or tablets[22].

PEG-diacrylate (PEGDA) hydrogels (Mr 575-20000) have mesh sizes less than 0.1-10 nm[15,29], which draws challenge because solutes with a hydrodynamic diameter comparable to the mesh size of the PEG network will not be able to diffuse into the center[30–32]. Thus, there exist critical needs for facile fabrication method for large mesh size and high porosity of hydrogel microparticles with controlled mesh sizes and structure.

To address the problem, porogen is often used to create pores. Kumacheva[33] and coworkers have used porogens encapsulated inside the monomer mix before polymerization in order to form porous and macroporous particles[6,33].

In this thesis, inert PEG600 is introduced as a porogen during polymerization.

2.1.4 Chitosan

Chitosan, a transformed oligosaccharide, is obtained by alkaline deacetylation of chitin. It has outstanding properties of nontoxicity, biocompatibility, biodegradability and low cost[34]. Chitosan has one primary amino and two free hydroxyl groups for each C_6 unit, which makes it a weak base and insoluble either in water or in organic solvents[35]. Nonetheless, it is soluble at low pH when its amine groups are protonated. In addition, chitosan's amine groups are more reactive in aqueous environments compared to other polyamines due to the low pK_a value of its primary amine[36], which makes it a perfect material to couple proteins onto.

Therefore, here in Chapter 3 of this thesis, chitosan is introduced to offer efficient handles for covalent binding via standard amine-reactive reactions.

2.1.5 Replica Molding Technique

There are a variety of methods established for the fabrication of hydrogel microparticles, which range from batch formats, such as photolithography or stop-flow lithography[4] to continuous formats, such as microfluidic devices[37].

Replica molding (RM)[11,38,39] is an efficient soft lithographic technique in which patterned molds are used to duplicate microstructures. This involves using microscale molds to create microparticles with very high resolution. Replica Molding (RM) involves three steps: i) creating a topographically patterned master; ii) transferring the pattern of this master into PDMS by replica molding; and iii) fabricating a replica of the original master by solidifying a liquid precursor against the PDMS mold[11].

Replica molding allows duplication of three-dimensional topologies in one single step. The particles can be controlled at a sub-micrometer level in a reliable and inexpensive way. Since RM has the advantages mentioned above, it has become a mass-production method of a wide range of structured surfaces such as compact disks (CDs), diffraction gratings, holograms, and micro-tools[38].

The RM technique with PDMS mold was applied for the PEG-Chitosan hydrogel microspheres fabrication in Chapter 3 of this thesis.

2.1.6 Polymerization-induced Phase Separation PIPS

Choi et al.[40] recently presented a new method of synthesizing spherical monodispersed particles through surface-tension-induced flow.

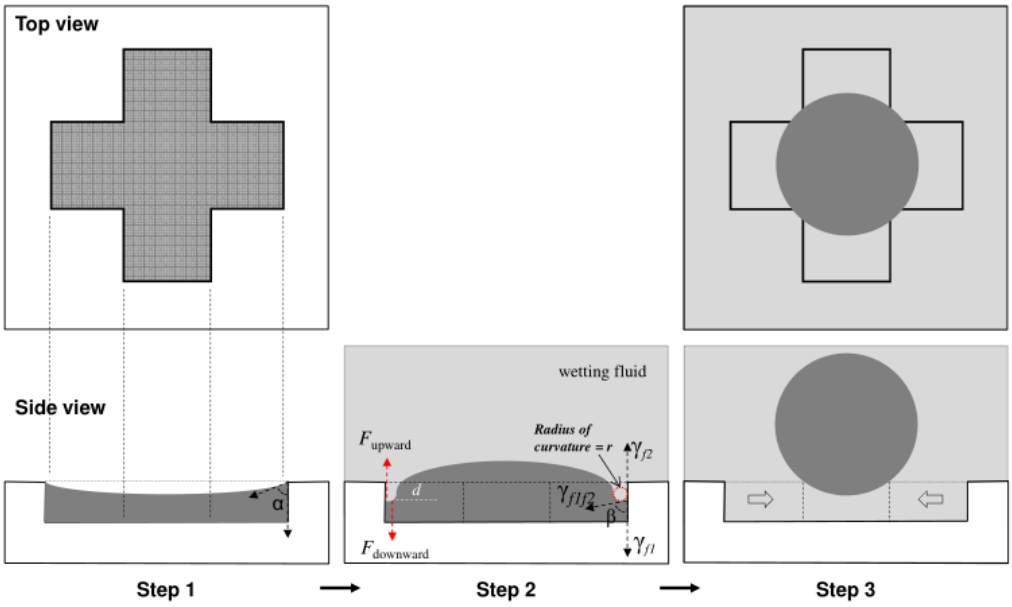

Figure 2.2. Schematic diagrams of the droplet formation, including wetting process (Step 1 and 2) and Laplace pressure driven flow process (Step 2 and 3)[40].

As indicated in Figure 2.2, the photocurable fluid is added to the PDMS mold with a contact angle α before the wetting fluid was applied (step 1).

Once wetting fluid was added, the pressure driving force due to the curvature of wetting fluid formed along edge of microwell (step 2), which leads the wetting fluid to move downward because F_{downward} is always greater than F_{upward} at any acute contact angle.

When the wetting solution reaches the vertices of the bottom of arm edge, the wetting step ends.

Significant difference of radius of curvature between edge of arms and center is provided by the natural geometry of cross-shape microwell. As a result, the Laplace pressure driven flow allows the photocurable fluid to move toward center and thus making formation of spherical droplet (step 3).

In this thesis, the PIPS-based synthesis method is utilized to fabricate the chitosan-PEG hybrid microspheres.

2.1.7 Michael Reaction

The Michael reaction or Michael addition is the nucleophilic addition of a carbanion or another nucleophile[41] to an α, β-unsaturated carbonyl compound. As shown in Scheme 2, first, hydroxide functions as a base and removes the acidic α-hydrogen giving the reactive enolate. Second, the nucleophilic enolate attacks the conjugated ketone at the electrophilic alkene C in a nucleophilic addition type process with the electrons being pushed through to the electronegative O, giving an intermediate enolate. Finally, an acid-base reaction occurs. The enolate deprotonates a water molecule recreating hydroxide and the more favorable carbonyl group.

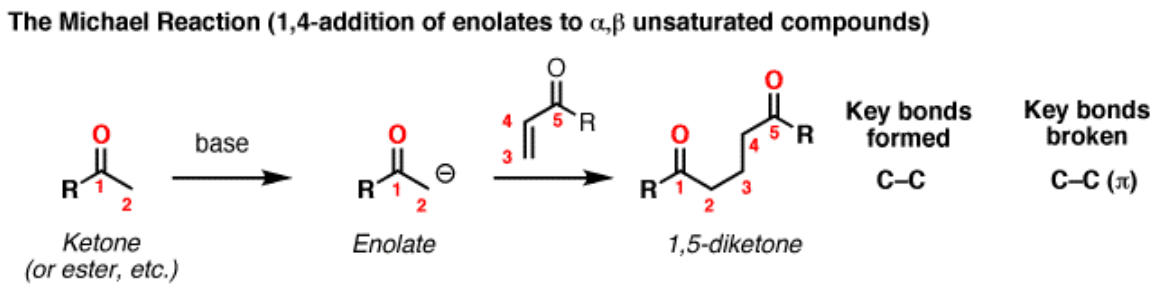

Scheme 2. The mechanism of Michael Reaction.[42]

2.2 Protein Conjugation

2.2.1 Tz-TCO reaction

To examine the utility of hydrogel microparticles, protein conjugation is one direct and efficient method, since protein-polymer conjugates impart a flexibility to their clinical usage[43]. Conjugation should enhance the properties of the protein, not increase its toxicity nor reduce its biological activity.

Heteroaromatic azadiene Diels−Alder reactions have become popular as bioorthogonal reactions towards conjugation due to their very fast "click-like" reactivity[44,45]. Karver et al.[46] have examined the rapid and bioorthogonal tetrazine (Tz)−trans-cyclooctene (TCO) cycloaddition reaction for labeling and confirmed its selectivity, high conjugation yield and stability of the functional groups.

In Chapter 3 of this thesis, Tz-TCO reaction is used to carry out protein conjugation towards the hydrogel microspheres.

3. Method and Materials

The materials and methods for the experiments in this thesis were similar to and slightly modified from a recent study by Jung and Yi[18].

3.1 Materials

Chitosan oligosaccharide lactate (average Mn 5 kDa, > 90% deacetylation), poly(ethylene glycol) diacrylate (PEGDA, average Mn 700 Da), poly(ethylene glycol) 600 (PEG 600, average Mn 600 Da), 2-hydroxy-2-methylpropiophenone (Darocur 1173, photoinitiator, PI), phosphate buffered saline (PBS) tablets (10 mM phosphate, 2.7 mM potassium chloride, 137 mM sodium chloride, pH 7.4), and saline sodium citrate (SSC) buffer (20× concentrate, molecular biology grade) were purchased from Sigma-Aldrich (St. Louis, MO). Red fluorescent protein R-Phycoerythrin (R-PE in sodium phosphate buffer, pH7.0 with ammonium sulfate) was purchased from AnaSpace (Fremont, CA). 5- (and 6-) carboxyfluorescein succinimidyl ester (NHS–fluorescein) was purchased from Pierce Biotechnology (Rockford, IL). Trans-cyclooctene (TCO)–PEG_4 –*N*-hydroxysuccinimide (NHS) ester, Tetrazine (Tz)–PEG_5 –NHS ester was purchased from Click Chemistry Tools (Scottsdale, AZ). NHS–PEG_{12} –azide, borate buffer (20× concentrate, 50 mM borate, pH 8.5), Tween 20 (TW20), poly(dimethylsiloxane) (PDMS) elastomer kits (Sylgard 184), and centrifugal filter units (Amicon Ultra 0.5) were purchased from Thermo Fisher Scientific (Waltham, MA). Dimethyl sulfoxide (DMSO, extra dry) and *N*-hexadecane (99%) were purchased from ACROS Organics TM. 2-propanol (> 99.7%) was purchased from J.T.Baker®. All the chemicals were analytical grade, and used without further purification.

3.2 Fabrication of Chitosan-PEG Microspheres

Chitosan-PEG Microspheres were fabricated via a simple and robust micromolding-based method as in a recent study[18]. First, a PDMS mold containing of 14x14 cross-shaped microwells was made via thermal curing of Sylgard 184 elastomer with 10% (w/w) crosslinking agent upon overnight incubation at 65 ℃ on a silicon master mold. Next, I prepared prepolymer solution by mixing chitosan (0.5 w/v), PEGDA (15-30% v/v), PEG600 (0-30%) and deionized (DI) water using vortex mixer (1 minute) and sonicator (10 minutes). The wetting fluid was prepared by mixing *N*-hexadecane with photoiniciator (PI, 1% v/v). The PDMS mold was covered with the prepolymer solution. The air bubbles were removed by scratching the mold with a disposable pipet tip so that the microwells were filled with prepolymer solution. The excess solution was taken away with a pipette, and the PDMS mold was covered with the wetting fluid. In order to prevent rapid evaporation of the prepolymer solution, the procedures mentioned above were carried out in a humidity chamber with over 90% humidity. The PDMS mold is not moved for 5 minutes as the droplets were forming because of the surface tension between the prepolymer solution and the wetting fluid. Afterwards, the droplets were cured with 365 nm UV light with an 8W hand-held UV lamp (Spectronics Corp., Westbury, NY) for 15 minutes for polymerization. The polymerized microspheres were then collected by pipetting and rinsed 5 times with 2-propanol, 3 times with DI water containing 0.5 (v/v) TW20, and 2 times with 5 × SSC buffer containing 0.05% (v/v) TW20 in order to get rid of any unreacted chemicals.

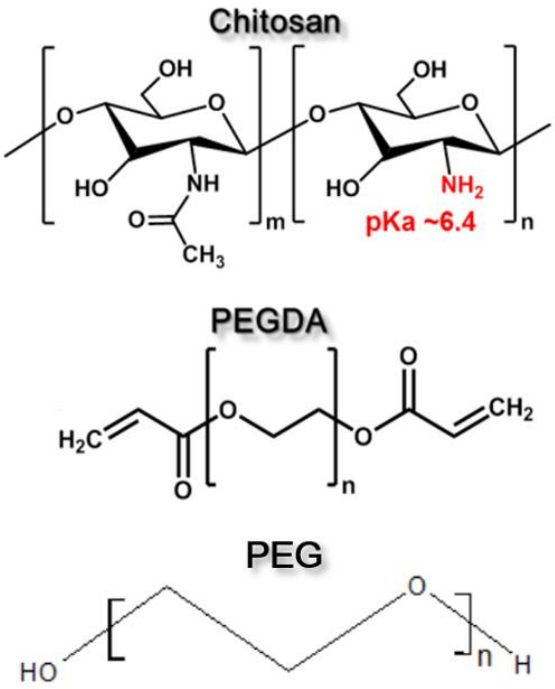

Figure 3.1 Chemical structures of chitosan, PEGDA and PEG[47]. In this thesis, chitosan lactate with MW 5kDa, PEGDA with MW 700 and PEG with MW 600 were used.

3.3 Fluorescent Labeling of Chitosan-PEG Microspheres

For fluorescent labeling, a constant number (~80) of CS-PEG microspheres were incubated in 5× SSC-TW20 buffer solution containing 10 μM of NHS-fluorescein for 1 hour on a rotator at room temperature covered with aluminum foil in order to avoid light exposure. The unreacted fluorescein residues were then separated by rinsing the microspheres 3 times with diluted 2-propanol (1:1 v/v mixture with DI water).

3.4 Azide-activation of R-PEs

To activate R-PEs with azide molecules, the buffer solution of the R-PE solution was exchanged with borate buffered saline (50 mM borate, 300mM NaCl, pH 8.5) via

centrifugal filtration at 4 ℃. The R-PEs were then reacted with 20-fold molar excess of NHS-PEG_{12}-azide for 30 minutes at room temperature. Unreacted chemicals were removed from the R-PE solution through centrifugal filtration (Amicon Ultra 0.5) with PBS buffer (pH 7.4). The concentration of the final Tz-activated R-PE solutions were measured by UV-vis spectrophotometry (EvolutionTM 300 UV-vis Spectrophotometer, Thermo scientific, Waltham, MA) with the characteristic absorbance peaks and molar extinction coefficients of the R-PE (1.96×10^6 $M^{-1}cm^{-1}$ at 565 nm).

3.5 R-PE Conjugation with Chitosan-PEG microspheres

In order to conjugate R-PE with the Chitosan-PEG microspheres, Tz-TCO cycloaddition reaction is utilized as shown in Figure 3.2. Specifically, a constant number (~80) of CS-PEG microspheres were first activated with TCO molecules upon 1-hour incubation with 500 μM TCO-PEG_4-NHS ester in 5× SSC buffer solution containing 0.05% (v/v) TW20 at room temperature, and washed 4 times with SSC-TW20 buffer. Then, TCO-activated CS-PEG microspheres were reacted with 2 μM Tz-activated R-PEs in SSC-TW20 buffer solution for 24 hours on a rotator at room temperature. At last, the unconjugated R-PEs were rinsed out by washing 5 times with SSC-TW20 buffer.

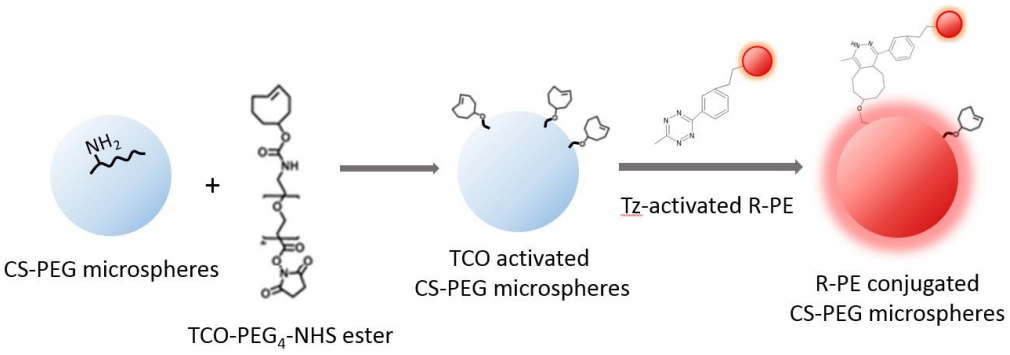

Figure 3.2. Schematic diagram for TCO activation of the CS-PEG microspheres via an amine-reactive chemistry and R-PE conjugation with the TCO-activated CS-PEG microspheres via Tz-TCO cycloaddition reaction, modified from Jung and Yi[48].

3.6 Scanning Electron Microscopy (SEM) Analysis

The Chitosan-PEG microspheres were first washed 3 times with DI water containing 0.5% (v/v) TW20 and 2 times with DI water in order to remove the remaining chemicals (e.g. salts in buffers). Next, the microspheres were freeze-dried for 24 hours in a lyophilizer (Labconco Corp., Kansas City, MO). The dry microspheres were then presented on a stub and sputter coated (The 108 Auto Sputter Coater, Ted Pella, Inc., Redding, CA) with a gold–palladium layer for 5 seconds. The morphology of the microspheres was characterized using a JEOL 5910 scanning electron microscope (SEM) operating at 5 kV.

3.7 Imaging Analysis

The microspheres were imaged with an epifluorescence microscope (Olympus BX51 equipped with a DP70 microscope digital camera, Center Valley, PA) using standard

green (U-N31001) and red (U-N31002) filter sets (Chroma Technology Corp., Rockingham, VT) for the fluorescein and the R-PEs, respectively. Confocal images were captured with a Leica DMIRE2 microscope equipped with a TCS SP2 scanner (Wetzlar, Germany), using a 20x objective at 488 nm and 543 nm excitation for the green fluorescent molecules and the R-PEs, respectively. Data of the microspheres (e.g. diameter, penetration depth) were analyzed with the image analysis software ImageJ[49].

4. Result and Discussion:

4.1 Simple Micromolding-Based Fabrication of Chitosan-PEG Microspheres with Core-shell Structure.

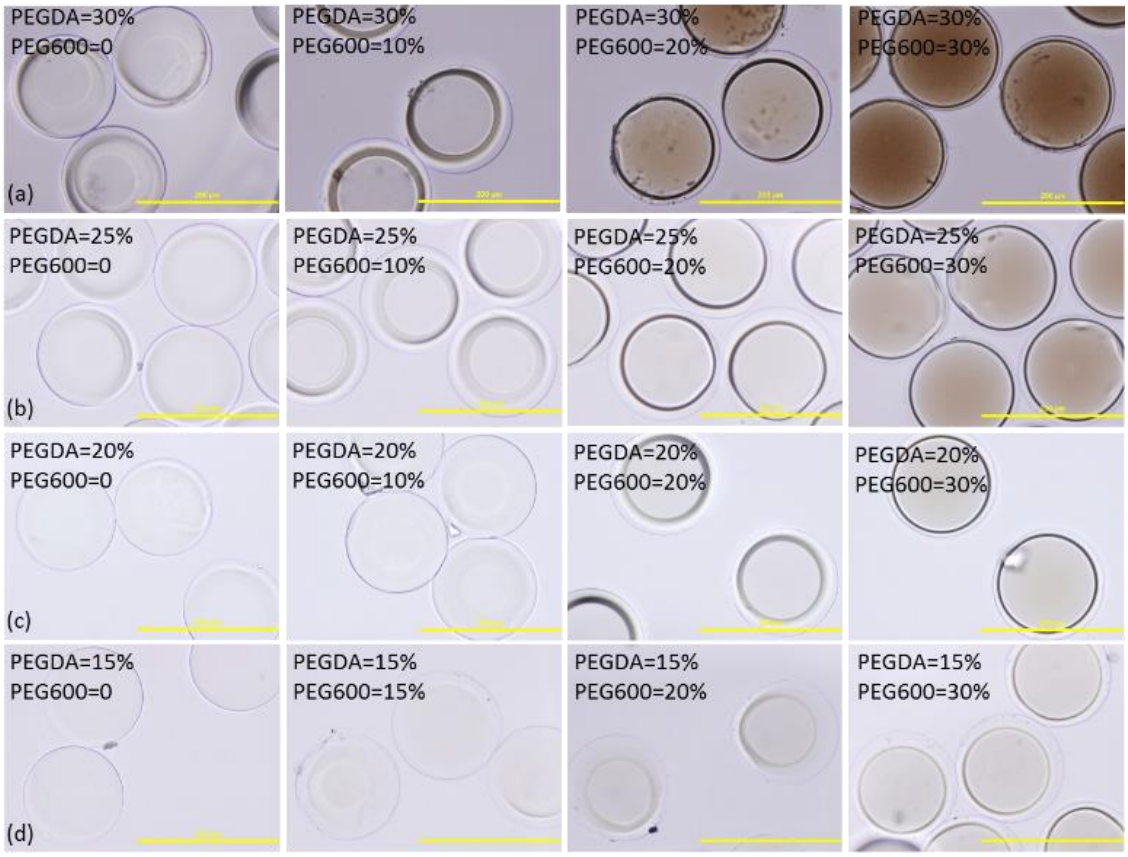

Figure 4.1. Bright-field micrographs of the chitosan-PEG microspheres fabricated with varying PEGDA concentrations (15-30%), varying PEG porogen concentrations (0-30%) and fixed chitosan content (0.5% w/v). Scale bars: 200 μm.

First, I examined the simple micromolding technique's utility to provide a robust method to fabricate highly uniform chitosan (CS)-PEG microspheres from various prepolymer compositions including the PEGDA and short chain PEG porogen (PEG 600), as shown in Figure 4.1.

For this, I first prepared the prepolymer solutions containing fixed concentration of 0.5% w/v chitosan and varying concentrations of PEGDA (15-30%) and PEG600 (0-30%). As shown in the schematic diagram of Scheme 1, I filled the cross-shaped PDMS micromold patterns with these prepolymer solutions, and poured the hydrophobic wetting fluid *N*-hexadecane containing 1% photoinitiator onto the PDMS mold to form droplets. After the droplet formation is complete, the mold is placed under UV light exposure for 15 minutes. Upon crosslinking via UV-irradiation, I collected and imaged the microspheres via brightfield microscopy.

First, the micrographs of Figure 4.1 show that the micromolding technique leads to uniform microspheres for all the prepolymer conditions examined. Most of the microspheres show more transparent outer area, suggesting less polymer content shell layers, as recently reported[18]. Such core-shell structure is observed in all the conditions except for low PEG content condition (15% PEGDA with no PEG600 porogen) as shown in the leftmost image of Figure 4.1d. For higher PEG content conditions, the boundary between the two layers of the core-shell structure becomes sharper and more distinct as shown in the rightmost column. In addition, for the same content of PEGDA, the more porogen is added, the more obscure and blurry the core region becomes. Note that the

microspheres prepared with 30% PEGDA for all the PEG600 porogen conditions (Figure 4.1a) as well as the 25% PEGDA with 20-30% PEG600 conditions (two rightmost images, Figure 4.1b) show dark color, suggesting the formation of macroporous network structures[18].

These results indicate that the CS-PEG microspheres with intermediate and various PEG porogen conditions can be readily prepared with the identical fabrication procedures. These brightfield images also show that most of the conditions may lead to the core-shell structures, consistent with a recent study[18]. Specifically, Jung and Yi showed that the CS-PEG microspheres prepared with 10% PEGDA don't form core-shell structures[18].

In short summary, the results shown in Figure 4.1 indicate that the chitosan-PEG microspheres with various prepolymer compositions can be fabricated reliably with the preparticle compositions examined, with most conditions showing signs of core-shell formation.

4.2 Swelling Ratio and Water Content of the Chitosan-PEG Hydrogel Microspheres Prepared with Varying Prepolymer Content.

I further examined the sizes and water contents of the microspheres using simple swelling ratio measurements, as shown in Table 4.1. The volumetric swelling ratio (*Q*) is calculated by:

$$Q = \frac{V_w}{V_d} \qquad (1)$$

Water content is calculated by:

$$\text{Water content} = \frac{V_W - V_D}{V_W} \qquad (2)$$

where V_W and V_D represent the volume of the microspheres under wet (swollen) and dry (shrunk) states, respectively.

Table 1. Swelling ratio and water content of the Chitosan-PEG hydrogel microspheres.

Condition(%)	Wet diameter (μm)	Dry diameter (μm)	Swelling ratio Q	Water Content
PEGDA=30, PEG600=0	153±3	105±0.7	3.09	67.70%
PEGDA=30, PEG600=20	170±2	104±2	4.37	77.10%
PEGDA=25, PEG600=0	149±2	105±0.7	2.85	65.00%
PEGDA=25, PEG600=10	157±1	104±2	3.41	70.90%
PEGDA=25, PEG600=20	164±2	108±1	3.53	71.40%
PEGDA=25, PEG600=30	169±2	107±3	3.98	74.60%
PEGDA=20, PEG600=0	154±2	95±0.5	4.22	76.50%
PEGDA=20, PEG600=10	162±2	98±2	4.53	77.90%
PEGDA=20, PEG600=20	167±2	99±3	4.74	79.20%
PEGDA=20, PEG600=30	174±2	100±2	5.35	81.00%
PEGDA=15, PEG600=0	146±4	86±1	5.72	79.60%
PEGDA=15, PEG600=15	151±4	87±2	5.22	80.90%
PEGDA=15, PEG600=20	155±3	86±1	5.89	82.30%
PEGDA=15, PEG600=30	155±2	87±2	5.72	82.90%

Briefly, for microspheres prepared from the same PEGDA content, the wet diameters increase with increasing PEG600 porogen content, while the dry diameters of these show minimal difference for most conditions. Moreover, for the low PEGDA conditions (15%), the swelling ratio stays around 5.2~5.9, showing minimal differences with varying PEG600 porogen. While under other conditions, there is a clear trend of increase in swelling ratio with the addition of PEG600 porogen. The water content of the microspheres ranges from 65.0% to 82.9%, depending on the PEGDA and PEG600 porogen conditions. For the same PEGDA content, high PEG600 porogen content provides the highest water content for all the conditions examined. This may be due to the varying crosslinking densities and polymer contents resulting from the different prepolymer concentrations.

4.3 Fluorescent Labeling of the CS-PEG microspheres

Next, I examined the chemical functionality and spatial distribution of the chitosan residues in the microspheres via simple fluorescent labeling, as shown in Figure 4.2.

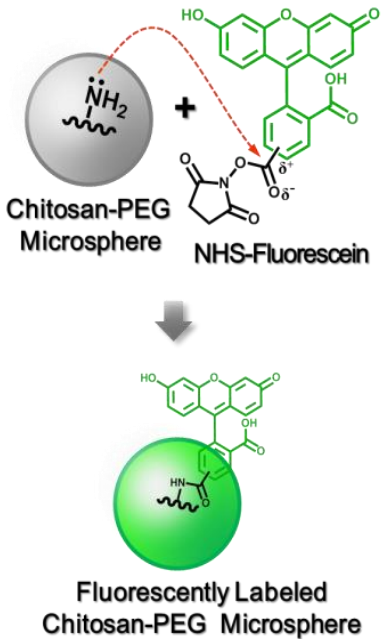

Figure 4.2. Schematic diagram for fluorescent labeling of the CS-PEG microspheres with NHS−fluorescein[18].

For this, I exposed the as-prepared microspheres fabricated with varying PEGDA and PEG600 porogen contents to an amine-reactive *N*-hydroxysuccimidyl ester form of carboxyfluorescein (NHS-fluorescein), and examined the resulting fluorescence from the amidation reaction via epifluorescence microscopy. For each condition, a fixed number of ~80 particles were incubated in SSC-TW20 buffer solution containing NHS-Fluorescein for 1 hour at room temperature, followed by 2-propanol - DI water (1:1v/v) washing step (5 times).

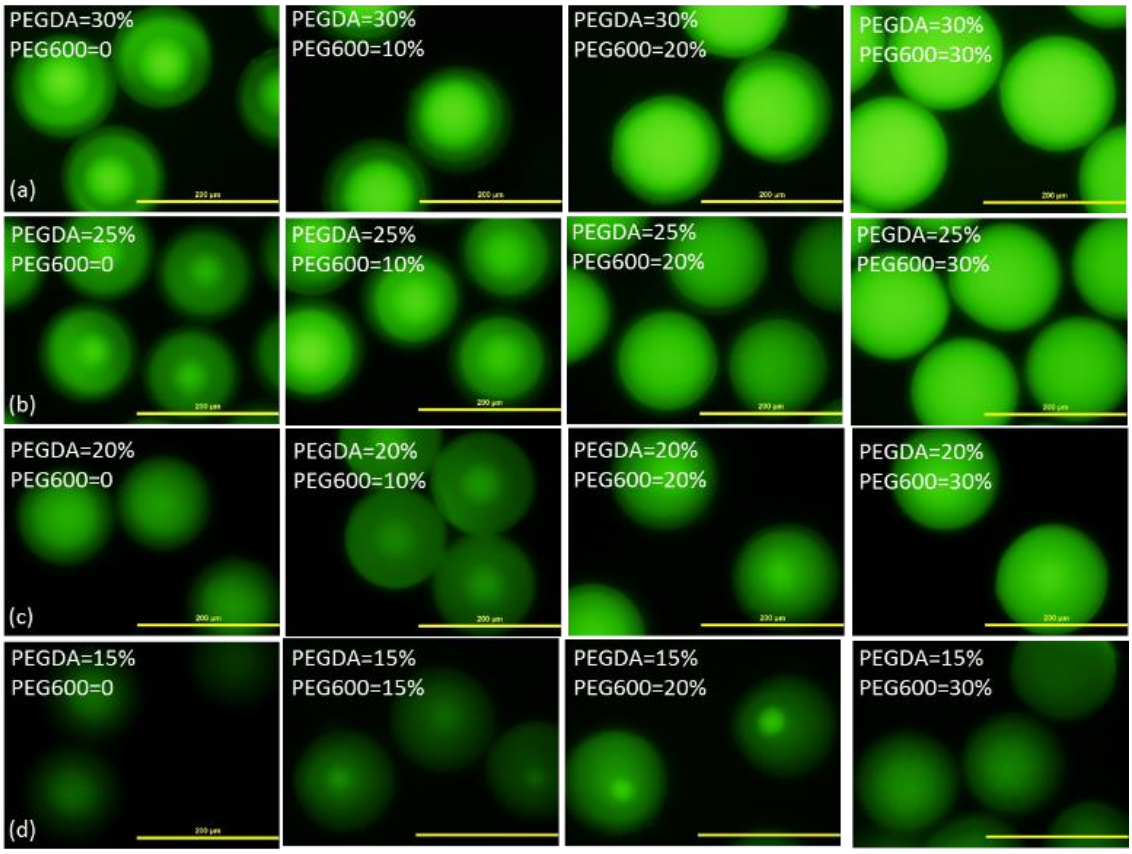

Figure 4.3. Fluorescence micrographs of the chitosan-PEG microspheres fabricated with varying PEGDA concentrations (15-30%), varying PEG porogen concentrations (0-30%) and fixed chitosan content (0.5% w/v). Scale bars: 200 μm.

First, the microspheres prepared with all the prepolymer conditions examined showed distinct fluorescence. Chitosan is a linear aminopolysaccharide composed of glucosamine monomer units with primary amine groups possessing a uniquely low pK_a value of ~6.4. This low pK_a makes chitosan's amine groups very reactive to standard amine-reactive chemistries, making it possible to examine the presence, distribution and chemical reactivity of chitosan via simple fluorescent labeling. As shown in Figure 4.2, the unshared electron pair of the amine group on chitosan attack the electron-deficient carbonyl carbon in the ester linkage of NHS-Fluorescein to form an amide bond via activated acyl substitution reaction, which leads to green fluorescent labeling of the microspheres[50]. Thus, the distinct fluorescence in the figures indicates a successful incorporation of chitosan onto the PEG microspheres. Meanwhile, microspheres prepared without chitosan showed minimal fluorescence, confirming the specific nature of the reaction (data not shown).

Next, the fluorescence images corresponding to the bright-field ones also show apparent core-shell structure, which indicates varying chitosan distribution in the microspheres. Specifically, the core regions of the microspheres for most conditions show brighter fluorescence, while the outer layers appear dim and dark, confirming the core-shell structures except for the 15 and 20% PEGDA – 30% PEG600 conditions.

Importantly, the fluorescein-labeled microspheres showed diverse fluorescence profiles depending on the prepolymer content. First, as shown in the leftmost column of Figure 4.3, microspheres prepared without PEG porogen showed core-shell like fluorescence,

while the ones prepared with 30% PEG600 porogen showed uniform fluorescence for all PEGDA content conditions (rightmost column).

When compared horizontally with constant PEGDA concentration condition, the overall and core regions' fluorescence of microspheres becomes brighter and the core region becomes larger. When compared vertically with the same PEG600 porogen content, the brightness of the microspheres increases with increasing PEGDA, accompanied by the expansion of the core region. This increase in fluorescence with identical chitosan content (0.5%) in the prepolymer solutions is likely due to enhanced polymerization and incorporation efficiency[51–53].

In short summary, the fluorescent labeling results in Figure 4.3 show that one can tune the distribution of the chemically reactive chitosan simply by modifying the prepolymer compositions.

4.4 The Spatial Distribution of Chitosan in CS-PEG Microspheres

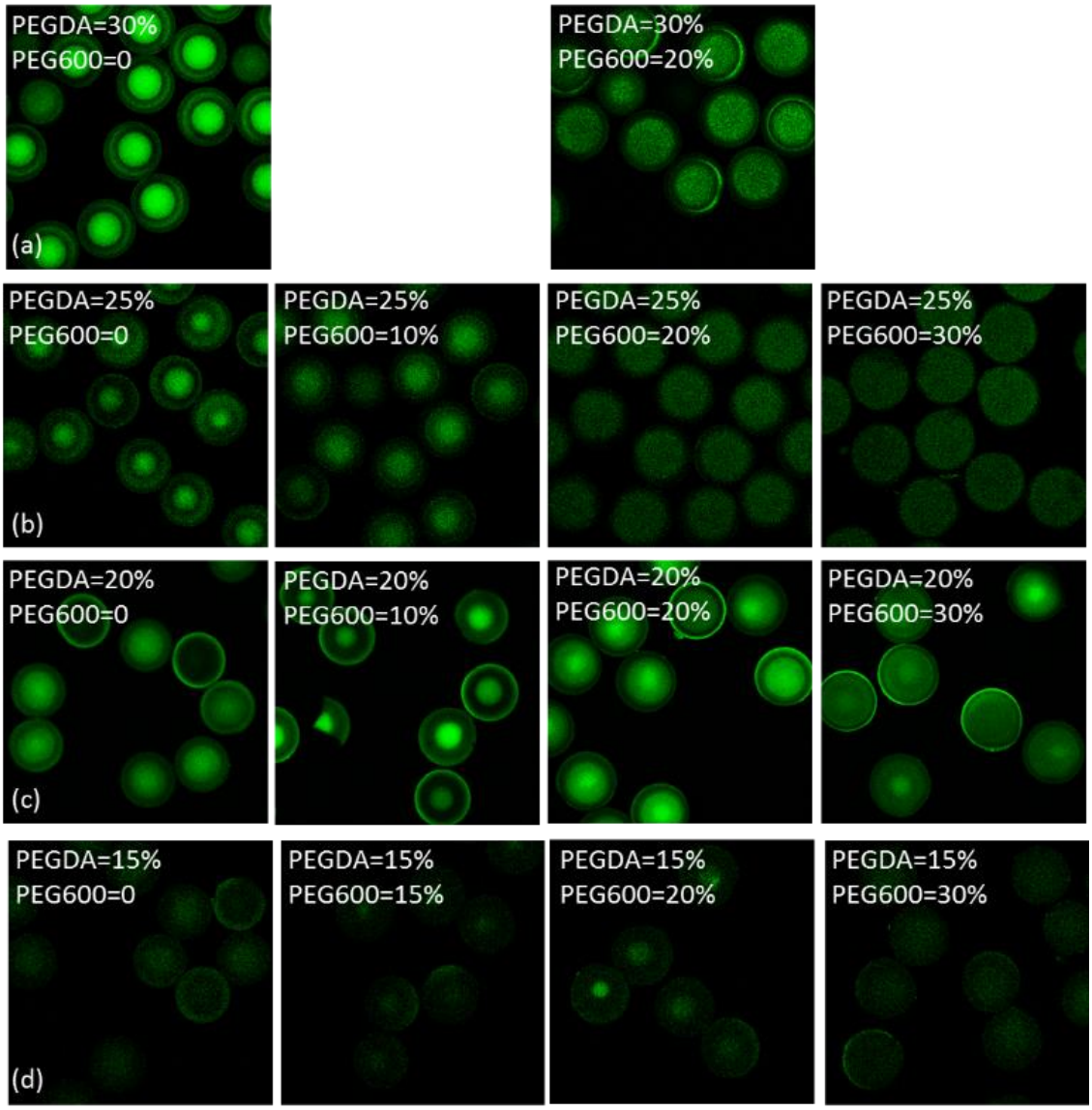

Figure 4.4. Confocal micrographs showing the distribution of chitosan within the fluorescent-labeled chitosan−PEG microspheres corresponding to the fluorescence micrographs of Figure 4.3.

In order to further examine the spatial distribution of chitosan, I then utilized confocal microscopy as shown in Figure 4.4.

For this, I imaged fluorescence of the middle plane of the fluorescein-labeled CS-PEG microspheres prepared with various PEGDA and PEG600 porogen contents using a confocal microscope. The micrographs are obtained with a 20x objective at 488 nm excitation.

First, most of the confocal images show that the small molecule fluorescein can penetrate through and react with chitosan within the microspheres' polymer networks. Also, the fluorescence (thus chitosan) distribution appear to correlate well between the epifluorescence (Figure 4.3) and confocal images (Figure 4.4). For example, fluorescence for microspheres prepared with 25% PEGDA and 0-10% PEG600 appear core-shell like, while the ones with 20-30% PEG600 appear more evenly distributed in both epifluorescence and confocal images. While confocal imaging conditions and results were not as quantitative as the epifluorescence results, the microspheres prepared with 15% PEGDA showed the least fluorescence for all PEG600 porogen conditions as shown in Figure 4.4(d). This result further confirms the epifluorescence results shown in Figure 4.3. When compared horizontally among same PEGDA contents, higher PEG600 porogen content appears to lead to more evenly distributed chitosan, as shown in the micrographs for 25% PEGDA and 20-30% PEG600 conditions.

Interestingly, one of the microspheres was broken (20% PEGDA, 10% PEG600), and the core-shell fluorescence distribution remained. This result indicates that chitosan is incorporated with the PEG network in a stable manner[47]. The stable incorporation is likely due to the covalent binding between the primary amine groups of chitosan and the acrylate groups of PEGDA via Michael addition reaction[41,42].

In short summary, the confocal imaging results in Figure 4.4 confirm various core-shell or uniform distribution of chitosan in the microspheres prepared with varying PEGDA and PEG content conditions.

4.5 Conjugation of R-PE with Chitosan-PEG Microspheres via Tz-TCO reaction

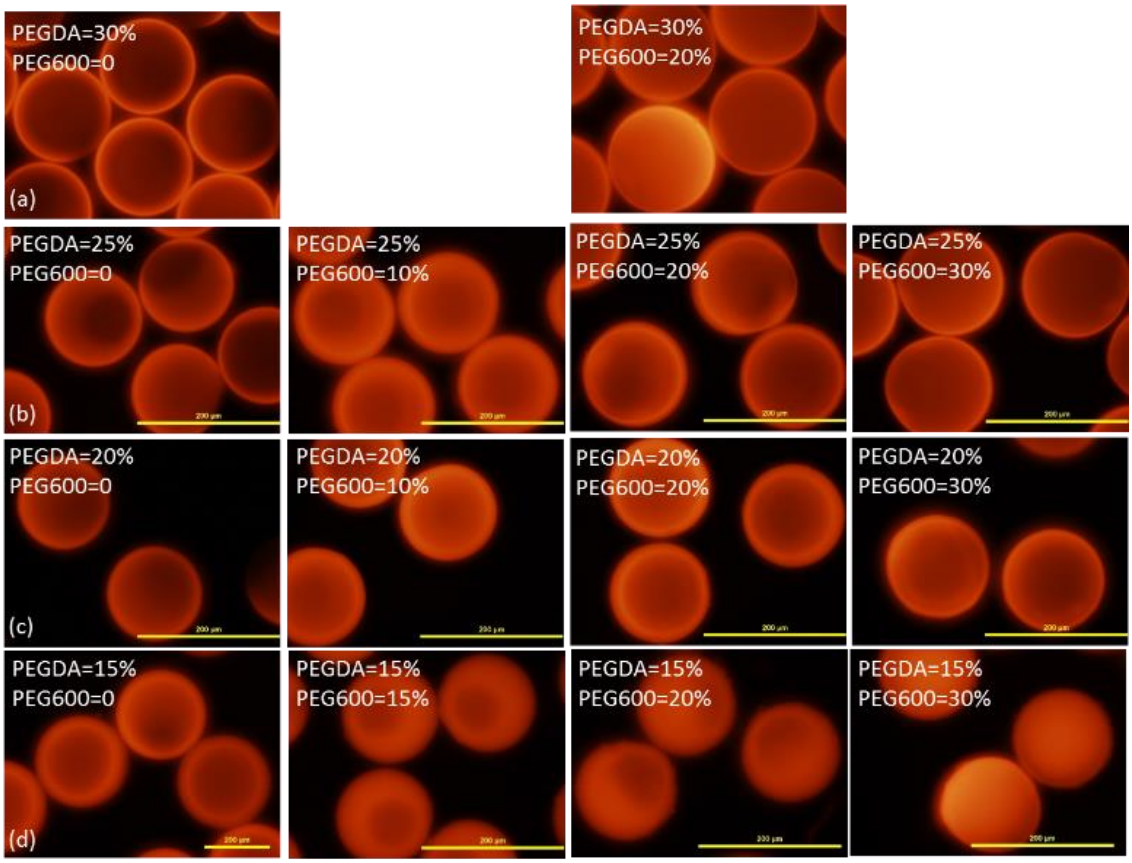

Figure 4.5. Fluorescence micrographs of R-PE conjugated chitosan-PEG microspheres with varying PEGDA concentrations (15-30%), varying PEG porogen concentrations (0-30%) and fixed chitosan content (0.5% w/v). Scale bars: 200 μm.

Conjugation of large proteins is the most direct and relevant means for examination of tunable macroporous polymer network structures toward biosensing applications. In Figure 4.5, I utilized conjugation of bright red fluorescent protein R-phycoerythrin (R-PE, M.W.= 240kDa, hydrodynamic diameter $D_h \approx 11$nm) to investigate the microspheres' network structures. For this, I used a high yield, rapid and biorthogonal Tetrazine-trans-cyclooctene (Tz-TCO) ligation reaction to conjugate the protein onto the microspheres.

Specifically, as shown in Figure 3.2, the as-prepared chitosan-PEG microspheres were first activated with TCO molecules for 1 hour at room temperature, then the TCO-activated CS-PEG microspheres were reacted with 2 μM of Tz-activated R-PE for 24 hours. The unreacted chemicals were removed by washing the microspheres with SSC-TW20 buffer for 5 times.

First, the fluorescence micrographs of Figure 4.5 show that the microspheres are successfully conjugated with R-PE in a core-shell distribution. These as-prepared microspheres have higher fluorescence intensity in the shell layer, suggesting the incomplete penetration of the R-PE biomolecules. For most of the images, the fluorescence concentrate in the outer surface of the microspheres, which correlates well with confocal imaging results below (Figure 4.6). As shown in the rightmost image of Figure 4.5(d), for microspheres prepared with low PEGDA (15%) and high PEG600 porogen content (30%), the fluorescence profile is different from the rest, for it shows uniform fluorescence intensity throughout the microspheres instead of near the surface.

Moreover, the overall fluorescence also suggests that PEG600 porogen occupies space within the hydrogel and does not have a tendency to denature proteins.

In contrast, minimal fluorescence is observed for negative controls (without TCO-activation), confirming selective conjugation of R-PE biomolecules with the microspheres (data not shown).

Overall, the results in Figure 4.5 show tunable and macroporous network structure of the microspheres applicable for biomacromolecular conjugation.

4.6 The R-PE conjugation within the CS-PEG Microspheres

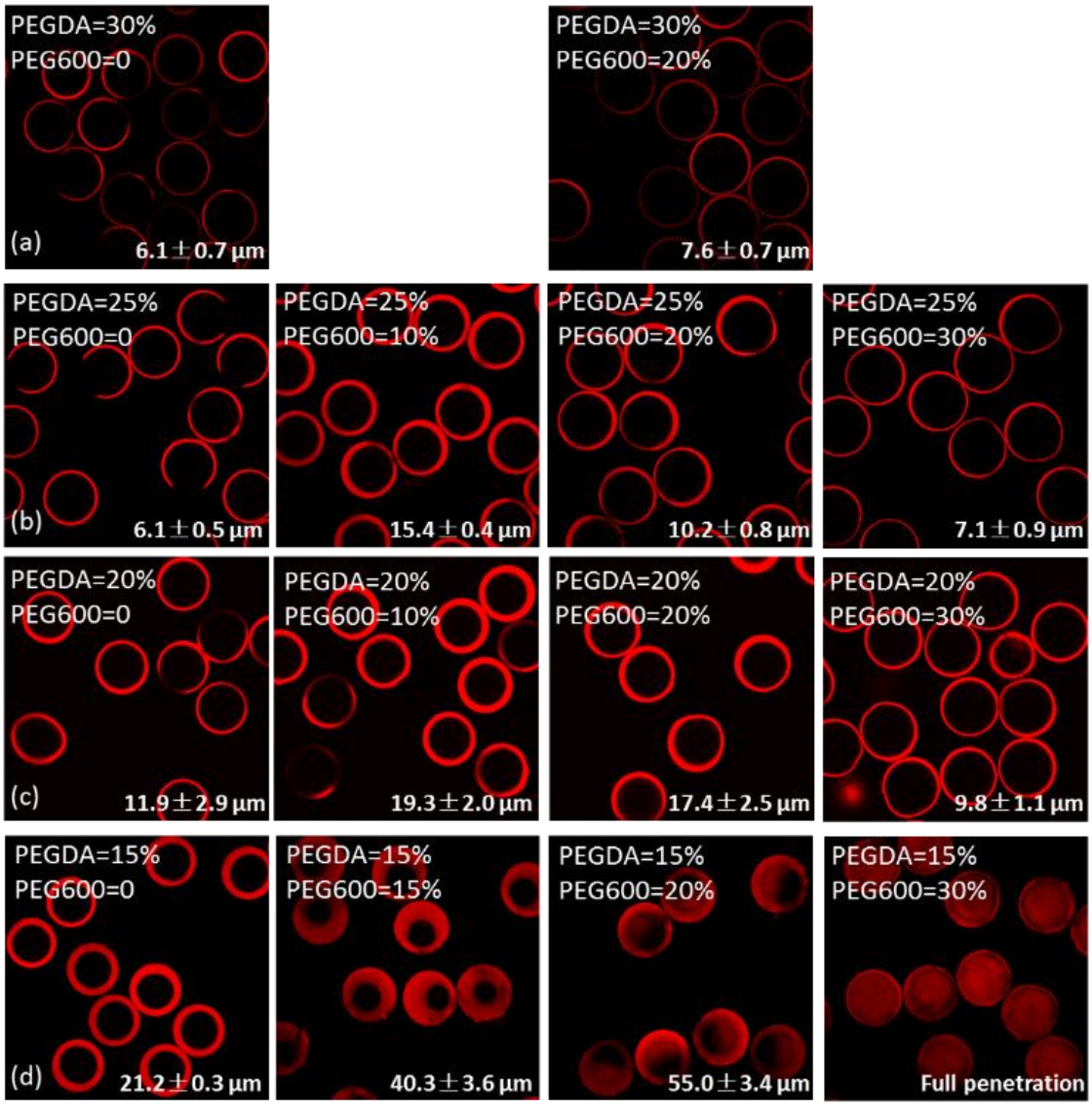

Figure 4.6. Confocal micrographs showing the R-PE penetration depth within the conjugated chitosan−PEG microspheres corresponding to the fluorescence micrographs of Figure 4.5.

I further examined the R-PE-conjugated microspheres via confocal microscopy as shown in Figure 4.6 in order to study the penetration depth of R-PE and the microspheres' 3D network structures in detail.

For this, the R-PE conjugated microshperes were imaged with a confocal microscope in SSC-TW20 buffer solution (pH 7.0). Confocal micrographs were obtained with a 20x objective at 543 nm excitation.

The confocal microscopy results taken at the center plane of the R-PE conjugated microspheres in Figure 4.6 show different fluorescence profiles and penetration depths depending on PEGDA and PEG600 porogen contents.

First, for most of the images, the fluorescence appears on the outer layer of the microspheres with well-defined penetration depths. These results are consistent with the epifluorescence result in Figure 4.5, confirming the core-shell structural features for most conditions.

Comparing vertically, the penetration depth increases with decreasing PEGDA content, indicating larger mesh size of the polymer network of the microspheres. For example, the penetration depth is about 6 ± 0.7 μm for the microspheres prepared with 30% PEGDA and no PEG600 porogen (top leftmost micrograph), and increases to average 21 ± 0.3 μm for the ones with 15% PEGDA (botton leftmost micrograph).

Comparing horizontally, increasing PEG600 porogen content does not appear to increase the penetration depth for most conditions. Specifically, 25% PEGDA condition showed 6.1 ± 0.5 μm of penetration depth without PEG600 porogen, which increased to 15 ± 0.4 μm at 10% PEG600 porogen condition, then decreased to 10 ± 0.8 μm and 7 ± 0.9 μm for the 20% and 30% PEG600 porogen condition. The fundamental mechanism of this lack of clear correlation is not clear at this point, while further conjugation kinetics study should provide more in-depth knowledge about the 3D structures of the microspheres' polymeric networks.

Interestingly, as shown in Figure 4.6(d), for microspheres prepared with 15% PEGDA, increased PEG600 porogen content leads to a thicker shell layer, resulting in complete penetration for 30% PEG600 condition. This result indicates that the formation of highly macroporous structures of the microspheres can be readily achieved, again by simply adding PEG600 porogen in the prepolymer solutions.

Table 2. Penetration depth of the R-PE within the R-PE conjugated CS-PEG microspheres prepared with varying PEG content.

Condition (%)	**Penetration depth (μm)**
PEGDA=30, PEG600=0	6 ±0.7
PEGDA=30, PEG600=20	8 ±0.7
PEGDA=25, PEG600=0	6 ±0.5
PEGDA=25, PEG600=10	15 ±0.4
PEGDA=25, PEG600=20	10 ±0.8
PEGDA=25, PEG600=30	7 ±0.9
PEGDA=20, PEG600=0	12 ±3
PEGDA=20, PEG600=10	19 ±2
PEGDA=20, PEG600=20	17 ±2
PEGDA=20, PEG600=30	10 ±1
PEGDA=15, PEG600=0	21 ±0.3
PEGDA=15, PEG600=15	40 ±4
PEGDA=15, PEG600=20	55 ±3
PEGDA=15, PEG600=30	Full penetration

Meanwhile, Table 2 summarizes the penetration depths measured from the images of the R-PE-conjugated microspheres shown in Figure 4.6. Note that for 15% PEGDA condition, the penetration depth increases with the addition of PEG600 porogen from 21 ± 0.3 μm (no PEG600 porogen) to a complete penetration (30% PEG600 porogen), while 15% and 20% PEG600 porogen conditions provide an intermediate penetration of 40 ± 4 μm and 55 ± 3 μm, respectively. This trend shows a clear impact of the PEG600 porogen, which could be used to readily control the macroporous structures of the microspheres for a variety of applications.

In short summary, the confocal imaging results on R-PE conjugated microspheres in Figure 4.6 and the penetration depth of R-PEs in Table 2 clearly demonstrate that the mesh size, R-PE penetration depths and overall 3D structures can be readily tuned by simple parameters in the prepolymer solution.

4.7 The SEM Result of the Polymer Network Mesh Size and Porous Feature Near the Surface of Chitosan-PEG Microspheres

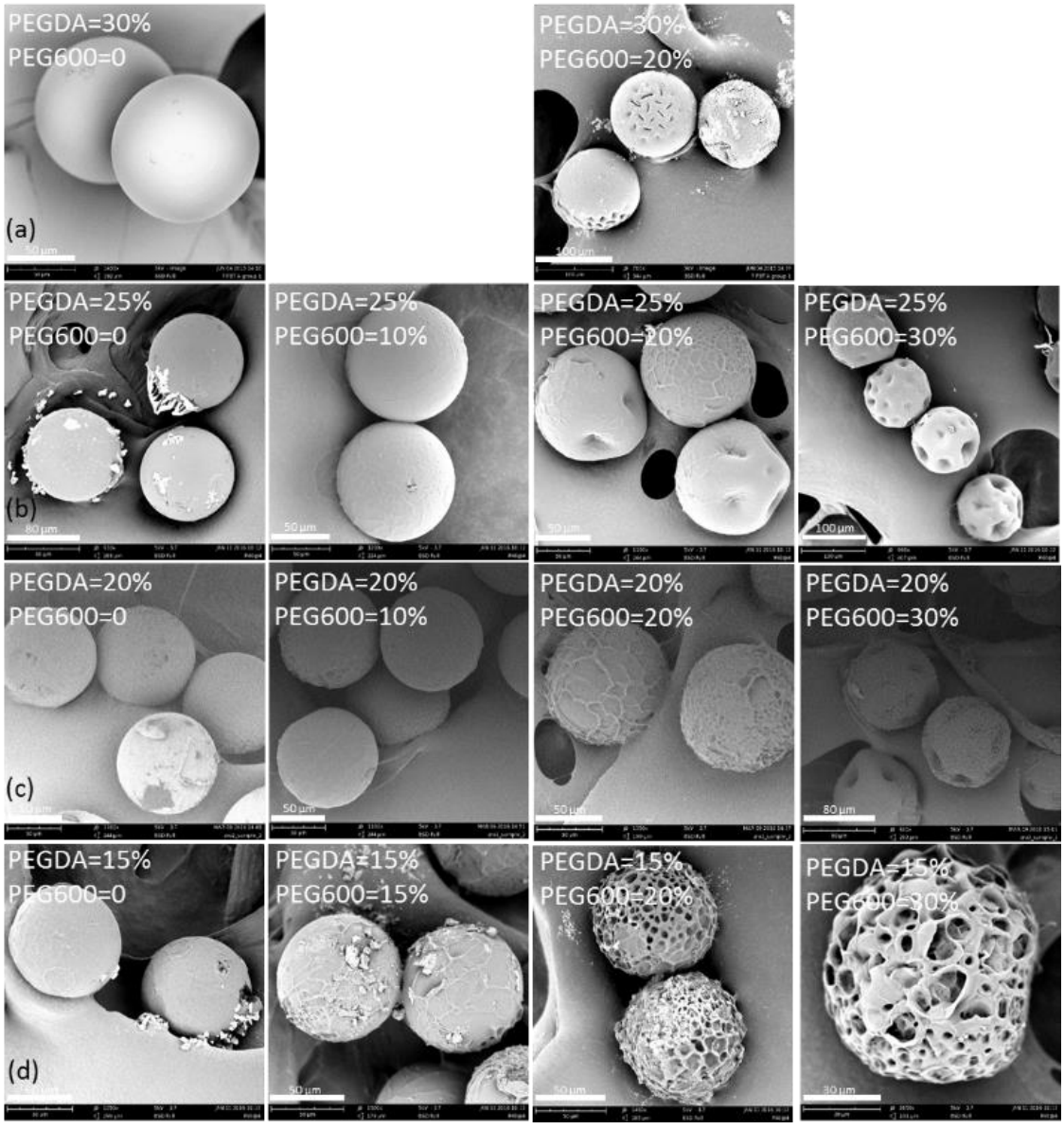

Figure 4.7. SEM micrographs of the lyophilized chitosan-PEG microspheres.

Next, I utilized scanning electron microscopy (SEM) to examine the structures and morphologies of the microspheres near their surfaces as shown in Figure 4.7.

For the SEM imaging, the remaining chemicals (e.g. salts in buffers) were removed by washing the as-prepared chitosan-PEG microspheres with DI water with TW20 (3 times) then with DI water only (2 times). Then, the microspheres were freeze-dried for 24 hours in a lyophilizer. The dry microspheres were then coated with a gold–palladium layer by a sputter coater for 5 seconds. The morphology of the microspheres was characterized using a scanning electron microscope (SEM) operating at 5 kV.

First, as shown in the leftmost column of Figure 4.7, the microspheres prepared with no PEG600 porogen show smooth surfaces. Comparing horizontally, as more PEG600 porogen was added, the surface of the microspheres becomes more wrinkled. Specifically, for Figure 4.7(b), 25% PEGDA with 0 or 10% PEG600 conditions showed no or little wrinkles on the surface, while the ones with 20% PEG600 condition appear to have more wrinkles. With the most porogen content (30% PEG600), the microspheres showed an interesting morphology with larger collapsed regions and holes on the surface as shown in the rightmost micrograph.

Comparing vertically, with the same PEG600 porogen content, Figure 4.7 showed a clear trend of increase in surface roughness with decreasing PEGDA content. For example, as shown in the third column of Figure 4.7, with the same PEG600 content added, the microspheres prepared with 30% PEGDA had a few cracks on the surface. As the

PEGDA content decreases, more wrinkles were observed, leading to an extensively wrinkled surfaces as shown in the bottommost micrograph. These wrinkles on the surfaces suggest that the outer shell regions of the microspheres prepared with high PEG600 porogen content may be highly macroporous with less crosslinked PEG structures, which collapsed to form the observed wrinkles during lyophilization. In other words, the wrinkles may suggest macroporous structure near the surface of the microspheres for some conditions. Thus, this difference in the microspheres morphology provided indirect evidence of PEG600 porogen's impact on how the polymer network structures form, including the mesh size and porous feature.

While technical difficulties in the sample preparation (e.g. shrinkage during lyophilization) made is very challenging to image the microspheres in states close to wet and swollen conditions, the SEM results provided useful information on the mesh sizes near the microsphere surfaces.

5. Conclusion:

In this thesis, I built on a recent study by Dr. Sukwon Jung [ref], and demonstrated a facile approach to fabricate chemically functional chitosan-PEG hybrid hydrogel microspheres with tunable macroporous structures utilizing biomolecular conjugation via bioorthogonal Tz-TCO cycloaddition reactions. First, the chitosan-PEG hydrogel microspheres with various prepolymer compositions were reliably fabricated via simple replica molding-based technique utilizing polymerization-induced phase separation, with most conditions showing signs of core-shell formation. Fluorescent labeling results showed stable incorporation of chitosan within the microspheres with a core-shell distribution and retained chemical functionality of the amine group. The biomolecular conjugation of R-PEs revealed tunable macroporous network structure which can be controlled simply by modifying the prepolymer compositions. Swelling ratio and scanning electron microscopy (SEM) studies also supported the tunable fabrication of the hybrid microspheres. I envision that the simple, robust, controllable and cost-efficient fabrication of hydrogel microspheres shown in this thesis can be enlisted in a wide range of biomolecular targets and medical applications.

6. Reference:

1. Uttamchandani, M., Neo, J. L., Ong, B. N. Z. & Moochhala, S. Applications of microarrays in pathogen detection and biodefence. *Trends in Biotechnology* **27,** 53–61 (2009).
2. Baker, K. N. *et al.* Rapid monitoring of recombinant protein products: a comparison of current technologies. *Trends Biotechnol.* **20,** 149–156 (2002).
3. Wulfkuhle, J. D., Liotta, L. a & Petricoin, E. F. Proteomic applications for the early detection of cancer. *Nat. Rev. Cancer* **3,** 267–275 (2003).
4. Dendukuri, D., Gu, S. S., Pregibon, D. C., Hatton, T. A. & Doyle, P. S. Stop-flow lithography in a microfluidic device. *Lab Chip* **7,** 818–828 (2007).
5. Pregibon, D. C., Toner, M. & Doyle, P. S. Multifunctional encoded particles for high-throughput biomolecule analysis. *Science* **315,** 1393–6 (2007).
6. Pregibon, D. C. & Doyle, P. S. Optimization of encoded hydrogel particles for nucleic acid quantification. *Anal. Chem.* **81,** 4873–4881 (2009).
7. Merkel, T. J. *et al.* NIH Public Access. *Langmuir* **26,** 13086–13096 (2011).
8. Meiring, J. E. *et al.* Hydrogel biosensor array platform indexed by shape. *Chem. Mater.* **16,** 5574–5580 (2004).
9. Teh, S.-Y., Lin, R., Hung, L.-H. & Lee, A. P. Droplet microfluidics. *Lab Chip* **8,** 198–220 (2008).
10. Utada, A. S. *et al.* Monodisperse Double Emulsions Generated from a Microcapillary Device. *Science.* **308,** 537–541 (2005).
11. Zhao, X.-M., Xia, Y. & Whitesides, G. M. Soft lithographic methods for nano-fabrication. *J. Mater. Chem.* **7,** 1069–1074 (1997).

12. Xu, S. *et al.* Erratum: Generation of monodisperse particles by using microfluidics - Control over size, shape, and composition. *Angewandte Chemie - International Edition* **44,** 3799 (2005).

13. Dendukuri, D., Tsoi, K., Hatton, T. A. & Doyle, P. S. Controlled synthesis of nonspherical microparticles using microfluidics. *Langmuir* **21,** 2113–2116 (2005).

14. Engberg, K. & Frank, C. W. Protein diffusion in photopolymerized poly(ethylene glycol) hydrogel networks. *Biomed. Mater.* **6,** 55006 (2011).

15. Cruise, G. M., Scharp, D. S. & Hubbell, J. A. Characterization of permeability and network structure of interfacially photopolymerized poly(ethylene glycol) diacrylate hydrogels. *Biomaterials* **19,** 1287–1294 (1998).

16. Hermanson, G. T. *Bioconjugate Techniques*. *Bioconjugate Techniques* (2013).

17. Welsch, N., Lu, Y., Dzubiella, J. & Ballauff, M. Adsorption of proteins to functional polymeric nanoparticles. *Polym. (United Kingdom)* **54,** 2835–2849 (2013).

18. Jung, S. & Yi, H. Facile Micromolding-Based Fabrication of Biopolymeric - Synthetic Hydrogel Microspheres with Controlled Structures for Improved Protein Conjugation. *Chem. Mater.* **27,** 3988–3998 (2015).

19. Young, R. J. & Lovell, P. A. *Introduction to Polymers, Third Edition*. (2011).

20. Odian, G. *Principles of Polymerization (3. Kapitel)*. *Principles of Polymerization, Fourth Edition* (2004). doi:10.1002/047147875X

21. Decker, C. Photoinitiated crosslinking polymerisation. *Prog. Polym. Sci.* **21,** 593–650 (1996).

22. Annabi, N. *et al.* 25th anniversary article: Rational design and applications of hydrogels in regenerative medicine. *Advanced Materials* **26,** 85–124 (2014).

23. Butun, S. & Sahiner, N. A versatile hydrogel template for metal nano particle preparation and their use in catalysis. *Polymer (Guildf).* **52,** 4834–4840 (2011).

24. Le Goff, G. C., Srinivas, R. L., Hill, W. A. & Doyle, P. S. Hydrogel microparticles for biosensing. *Eur. Polym. J.* **72,** 386–412 (2015).

25. Hoare, T. R. & Kohane, D. S. Hydrogels in drug delivery: Progress and challenges. *Polymer* **49,** 1993–2007 (2008).

26. Slaughter, B. V, Khurshid, S. S. & Fisher, O. Z. Hydrogels in Regenerative Medicine. *Advanced Materials* **21**, 3307-3329 (2009).

27. Léger, B., Menuel, S., Ponchel, A., Hapiot, F. & Monflier, E. Nanoparticle-based catalysis using supramolecular hydrogels. *Adv. Synth. Catal.* **354,** 1269–1272 (2012).

28. Sun, X. F., Jing, Z. & Wang, G. Preparation and swelling behaviors of porous hemicellulose-g-polyacrylamide hydrogels. *J. Appl. Polym. Sci.* **128,** 1861–1870 (2013).

29. Lee, A. G., Arena, C. P., Beebe, D. J. & Palecek, S. P. Development of macroporous poly(ethylene glycol) hydrogel arrays within microfluidic channels. *Biomacromolecules* **11,** 3316–3324 (2010).

30. Canal, T. & Peppas, N. a. Correlation between mesh size and equilibrium degree of swelling of polymeric networks. *J. Biomed. Mater. Res.* **23,** 1183–1193 (1989).

31. Mellott, M. B., Searcy, K. & Pishko, M. V. Release of protein from highly cross-linked hydrogels of poly(ethylene glycol) diacrylate fabricated by UV polymerization. *Biomaterials* **22,** 929–941 (2001).

32. Russell, R. J., Axel, A. C., Shields, K. L. & Pishko, M. V. Mass transfer in rapidly photopolymerized poly(ethylene glycol) hydrogels used for chemical sensing. *Polymer (Guildf).* **42,** 4893–4901 (2001).

33. Dubinsky, S. *et al.* Microfluidic synthesis of macroporous copolymer particles. *Macromolecules* **41,** 3555–3561 (2008).

34. Xu, J. H., Zhao, H., Lan, W. J. & Luo, G. S. A novel microfl uidic approach for monodispersed chitosan microspheres with controllable structures. *Adv. Healthc. Mater.* **1,** 106–111 (2012).

35. Ravindra, R., Krovvidi, K. R. & Khan, A. A. Solubility parameter of chitin and chitosan. *Carbohydr. Polym.* **36,** 121–127 (1998).

36. Yi, H. *et al.* Chitosan scaffolds for biomolecular assembly: Coupling nucleic acid probes for detecting hybridization. *Biotechnol. Bioeng.* **83,** 646–652 (2003).

37. Lee, A. G., Beebe, D. J. & Palecek, S. P. Quantification of kinase activity in cell lysates via photopatterned macroporous poly(ethylene glycol) hydrogel arrays in microfluidic channels. *Biomed. Microdevices* **14,** 247–257 (2012).

38. Xia, Y. & Whitesides, G. M. Soft Lithography. *Annu. Rev. Mater. Sci.* **28,** 153–184 (1998).

39. Xia, Y. *et al.* Complex Optical Surfaces Formed by Replica Molding Against Elastomeric Masters. *Science* **273,** 347–349 (1996).

40. Choi, C. H., Jeong, J. M., Kang, S. M., Lee, C. S. & Lee, J. Synthesis of monodispersed microspheres from laplace pressure induced droplets in micromolds. *Adv. Mater.* **24,** 5078–5082 (2012).

41. Little, D. R., Masjedizadeh, M. R., Wallquist, O. & McLoughlin, J. I. in *Organic reactions* 316 – 543 (1995).

42. Mather, B. D., Viswanathan, K., Miller, K. M. & Long, T. E. Michael addition reactions in macromolecular design for emerging technologies. *Progress in Polymer Science (Oxford)* **31,** 487–531 (2006).

43. Katre, N. The conjugation of proteins with polyethylene glycol and other polymersAltering properties of proteins to enhance their therapeutic potential. *Adv. Drug Deliv. Rev.* **10,** 91–114 (1993).

44. Talbot, A. *et al.* Activation-Strain Analysis Reveals Unexpected Origin of Fast Reactivity in Heteroaromatic Azadiene Inverse-Electron-Demand Diels-Alder Cycloadditions. *J. Org. Chem.* **80,** 548–558 (2014).

45. Hu, J. *et al.* Photonic crystal hydrogel beads used for multiplex biomolecular detection. *J. Mater. Chem.* **19,** 5730 (2009).

46. Karver, M. R., Weissleder, R. & Hilderbrand, S. A. Bioorthogonal reaction pairs enable simultaneous, selective, multi-target imaging. *Angew. Chemie - Int. Ed.* **51,** 920–922 (2012).

47. Jung, S. & Yi, H. Fabrication of chitosan-poly(ethylene glycol) hybrid hydrogel microparticles via replica molding and its application toward facile conjugation of biomolecules. *Langmuir* **28,** 17061–17070 (2012).

48. Jung, S. & Yi, H. An integrated approach for enhanced protein conjugation and capture with viral nanotemplates and hydrogel microparticle platforms via rapid bioorthogonal reactions. *Langmuir* **30,** 7762–7770 (2014).

49. Rasband, W. ImageJ 1997-2012. *U. S. National Institutes of Health, Bethesda, Maryland, USA* (2012).

50. Wade, L. G. *Organic Chmistry*. (Pearson Education: Upper Saddle River, 2003).

51. El-Sherbiny, I. M. & Smyth, H. D. C. Poly(ethylene glycol)-carboxymethyl chitosan-based pH-responsive hydrogels: Photo-induced synthesis, characterization, swelling, and in vitro evaluation as potential drug carriers. *Carbohydr. Res.* **345,** 2004–2012 (2010).

52. El-Sherbiny, I. M. Synthesis, characterization and metal uptake capacity of a new carboxymethyl chitosan derivative. *Eur. Polym. J.* **45,** 199–210 (2009).

53. Sabaa, M. W., Mohamed, N. A., Mohamed, R. R., Khalil, N. M. & Abd El Latif, S. M. Synthesis, characterization and antimicrobial activity of poly (N-vinyl imidazole) grafted carboxymethyl chitosan. *Carbohydr. Polym.* **79,** 998–1005 (2010).